Enhanced functional properties of CeO_2 modified graphene/epoxy nanocomposite coating through interface engineering

Ying Qian[1], Wei Zheng[1,3], Wenge Chen [1 *], Tao Feng[1],

Terence Xiaoteng Liu,[2] Yong Qing Fu[2 *]

[1] School of Materials Science and Engineering, Xi'an University of Technology, Xi'an, Shaanxi, 710048, P.R. China.

[2] Faculty of Engineering and Environment, Northumbria University, Newcastle upon Tyne, NE1 8ST, UK.[1]

[3] Xi'an Huichuang Research Institute for Precious Metal New Materials, Xi'an, Shaanxi, 71000, P.R. China.

Abstract: This paper reports significant enhancement of corrosion resistance and electrical properties of waterborne epoxy coatings through additions of ceria modified graphene. Results showed that ceria particles were uniformly distributed and covalently bonded onto the surface of graphene. A dense interface layer was formed between the ceria modified graphene and epoxy matrix by aliphatic ether bonds. The composite coating with a modified graphene content of 0.5 wt.% exhibited the best corrosion resistance with the highest impedance modulus (e.g., $10^3\ \Omega cm^2$ for the damaged coating) and the lowest corrosion rate (e.g., 0.002 mm/year). The excellent corrosion resistance of the composite coating is related to the barrier effect of graphene and the inhibition effect of ceria on metal corrosion. Moreover, the coating showed a low percolation threshold of 0.231 vol.% and its electrical conductivity reached 10^{-5} S/m when the content of modified graphene was 0.5 wt.%.

[1] Corresponding authors: Professor Wenge Chen; Prof.Richard Y.Q.Fu.
E-mail: wgchen001@263.net (W.G. Chen), richard.fu@northumbria.ac.uk (Richard Y.Q. Fu)

Keyword: Graphene; Epoxy resin; Corrosion resistance; Corrosion resistance; Conductivity

1. Introduction

Corrosion is one of the main failure modes of metals, and the cost due to damage or economic loss caused by corrosion of metals can be up to trillions of dollars annually [1]. Among various anti-corrosion technologies, protective coatings are widely used because of their convenient applicability, wide adaptability, and low repair cost. Epoxy resin is a class of polymer commonly used in anti-corrosion coatings due to its high adhesion strength, chemical resistance, and good insulation [2]. However, since most waterborne coatings for environmental protection use water as the dispersion medium, the residual hydrophilic groups in the coating will form water permeation channels which affect the corrosion resistance of the coating [3]. Meanwhile, industry applications often require coatings to have multiple functions [4,5], such as antistatic property [6,7] for electromagnetic interference [8,9], and self-cleaning [10] for protection and decoration. In this regard, many carbon-based nanofillers, such as carbon nanotubes [11], carbon black [12], graphene oxide (GO) and graphene [13,14], have been explored to use in these composite coatings.

Graphene is a two-dimensional nanomaterial with a single layer of ~0.35 nm [15]. It has extremely high tensile strength (~130 GPa), Young's modulus (~1.0 TPa) [16], high electrical conductivity (~10^8 Sm^{-1}) [17], thermal conductivity (5300 $Wm^{-1}K^{-1}$) [18] and large specific surface area (2630 m^2g^{-1}) [19]. If the appropriate amount of graphene is added into the coating, the layered graphene will be embedded inside the coating and filled with defects. This will delay the penetration of corrosive medium, form physical barriers to the corrosive medium, and improve the corrosion resistance of the coating. If graphene fillers can be homogeneously dispersed in the coating and then connected into continuous paths, the electrical conductivity

of coating can be greatly enhanced [20,21]. However, it is a huge challenge to find an appropriate process to disperse graphene uniformly into epoxy matrix. Chang et al. [22] previously prepared graphene/epoxy composite coatings with a unique bionic structure using a nano-casting technology. The coating surface has a good superhydrophobic property, with a good protection effect on the cold rolled steel. At present, a commonly used method is to functionalize the surface of graphene with small organic molecules, polymers, and inorganic non-metallic compounds. For example, Pourhashem et al. [23] prepared the composite coating by *in-situ* mixing silica modified graphene and epoxy and the coating showed an excellent corrosion resistance with the corrosion rate decreased from 0.1705 mm/year to 0.0012 mm/year. Ramezanzadeh et al. [24] filled 3-aminopropyltriethoxysilane grafted graphene oxides into silicon alkyl epoxy and prepared composite materials using a sol-gel method, thus enhancing the corrosion protection and stripping resistance of the epoxy coating. Jiang et al. [25] chemically grafted multi-walled carbon nanotubes onto p-phenylenediamine (PPD) modified GOs, and then used them as conductive fillers to prepare graphene/epoxy resin composite coating, achieving excellent electrical conductivity and corrosion resistance. Zhan et al. [26] modified GO/Fe_3O_4 hybrids with dopamine (DA) and 3-aminopropyltriethoxysilane (KH550) using a hydrothermal method and then filled with epoxy resin to prepare GO- Fe_3O_4-KH550/DA composite coatings. The composite coating exhibited excellent corrosion resistance and high hardness when the mass fraction of the filler was 0.5 wt.%.

Although there are a lot of studies on the graphene based composite coatings, the structures and properties of intrinsic graphene are easily changed during its modification process. Rare earth elements such as Ce are normally chemically active and have strong affinities with C, H, O, N, and other non-metallic elements. They can be combined with the graphene and GO to reduce the surface energy and improve its dispersion and functional properties of the component [27]. However, there are few previous studies for the rare earth element modified graphene/resin

composite coatings.

In this paper, we propose a new coating protection mechanism that uses metal cations to form a passivation layer under the coating. We then prepare the CeO_2@rGO/EP composite coating and study its electrochemical performances. Ceria modified graphene oxides were firstly prepared using a two-step reduction method of hydrothermal and calcination. They were then introduced into epoxy coating and brushed onto Q235 steel plate with a bar coater. We further studied the binding of graphene oxide, ceria, and epoxy resin, and the interface structures of the composite coating. Finally, the corrosion resistance and mechanisms of the composite coating were systematically investigated.

2. Protection mechanism of composite coating

The design mechanism for the ceria modified graphene and the enhanced protection principle of the composite coating are illustrated in Fig. 1. H_2O, O_2 molecules and Cl^- ions in the corrosion medium diffuse and permeate into the epoxy/steel interface along the micropores and defects in the coating (as shown in Fig. 1a). The graphene nanosheets modified by ceria can be dispersed uniformly in the epoxy matrix, thus acting as a barrier for defects (as shown in Fig. 1b). Once the corrosion medium contacts with the matrix, the redox reactions at the coating/metal interface will occur, and the reaction processes are shown below [28]:

$$Fe \rightarrow Fe^{2+} + 2e^- \quad (1)$$

$$Fe^{2+} \rightarrow Fe^{3+} + e^- \quad (2)$$

$$2H_2O + O_2 + 4e^- \rightarrow 4OH^- \quad (3)$$

$$2Fe^{2+} + O_2 + 2H_2O \rightarrow 2FeOOH + 2H^+ \quad (4)$$

Due to the excellent conductivity of graphene, in the above reaction processes, the

graphene can act as a cathode and the metal as an anode, thus forming a micro-environment to accelerate the electrochemical corrosion rate of the matrix. As the content of graphene filler is increased, more galvanic couples are formed at the coating/matrix interfaces which can speed up the metal corrosion.

【Insert Figure 1】

However, when the graphene is modified with ceria, the cerium could be quickly released into the NaCl electrolyte due to the cation exchange mechanism [29]. The sodium ions in the electrolyte that permeate into the epoxy coting can be replaced by Ce^{3+} ions on the modified graphene nanosheets. Previous studies reported that the cations such as zinc and cerium can react and form the chemical conversion coating or adsorption protective film [29–31] on the metal surface. Therefore, the Ce^{3+} ions could restrain the electrochemical corrosion of the substrate by forming the conversion coating under the epoxy, thus significantly improving the corrosion resistance.

3. Experimental

3.1. Materials

Graphene oxide prepared using the Hummer method was supplied by the Shaanxi Coal Chemistry New Energy Materials Research Institute, China. Cerium chloride heptahydrate was supplied by the Shanghai Sinochem Reagent Co. LTD, China. Waterborne epoxy resin (bisphenol A, E-44), defoamer and coalescing agent, were obtained from Shenzhen Jitian Chemical Co. LTD, China. All the chemicals were directly used without further treatment. The substrate was the Q235 carbon steel, and the dimension of carbon steel sample was 80 nm×40 nm×2 mm. The main chemical elements of the steel are listed in Table 1.

【Insert Table 1】

3.2. Preparation of filler and coating

Graphene oxide was added into deionized water followed by ultrasonic mixing for 2 hours to obtain a 2 mg/ml GO aqueous solution. 40 ml of GO aqueous solution was mixed with 40 ml of cerium chloride heptahydrate solution (a concentration of 2.4 mmol/L) to achieve a solution, which was continuously stirred for 3 hours. The solution was kept for 24 hours to ensure Ce^{3+} ions embedded with GO sheets uniformly. Then the mixture was transferred into a Teflon high-pressure reactor and heated for 12 hours at 120 ℃. The reactor was cooled down to room temperature. The solution was dialyzed to neutral with deionized water, and freeze-dried to obtain the rGO precursor with Ce^{3+} ions on its surface (e.g., formation of Ce^{3+}@rGO). Finally, the precursor powder was heat treated at 750 ℃ in a nitrogen atmosphere for one hour and cooled down within the furnace to obtain the rare earth modified graphene powder (e.g., CeO_2@rGO).

Different weight ratios of graphene powders (0 wt.%, 0.25 wt.%, 0.5 wt.%, 0.75 wt.%, 1.0 wt.%) were added into deionized water under a continuous ultrasonic agitation for one hour, and then mixed with waterborne epoxy and wetting dispersant under a constantly ultrasonic stirring for another one hour at room temperature. The curing agent, defoamer and coalescing agent were then added, and the modified graphene/epoxy composite coating was obtained after 10 min of stirring until a homogeneous solution was obtained. The solid content of the whole coating system was about 60%. The mixture was coated onto the Q235 steel using a bar coater to obtain a layer thickness of 100 μm, and then cured at 65 ℃ for one hour. This is followed by another coating process, then finally cured at 65 ℃ for 12 hours. For a comparison, 0.5 wt.% graphene/epoxy composite coating was also prepared using the same method.

3.3. Characterization

Crystalline structure of rare earth modified graphene was analyzed using an X-ray diffractometer (XRD-7000) with Cu Kα targets (λ=0.154 nm) at a voltage of 40 kV and a current of 40 mA. Microstructures of the modified graphene were observed using a transmission electron microscope (TEM，FEI-Talos，F200X). Changes in the composition, chemical state and oxygen-containing functional groups of the modified graphene were measured by X-ray photoelectron spectroscopy (XPS, AXIS ULTRA) in the energy range of 0~1200 eV. The collect data were processed with Casa XPS software for peak splitting and data Gaussian fitting.

Elemental bonding for the prepared coatings was studied using a TENSOR 27 Fourier Transform Infrared spectrometer (FT-IR). Cross-section morphology of the coating was observed using a scanning electron microscope (SEM, TESCAN VEG3XMU). Microscale topography of the composite coatings were obtained using TEM.

Hardness of the coatings was obtained using a Shore A hardness tester. Electrochemical tests were carried out using a P4000 electrochemical work station with a three-electrode system. A platinum electrode and saturated calomel electrode were served as the counter and reference electrodes, respectively, while the sample was used as the working electrode with 1 cm^2 active working area. The electrochemical tests were performed after the open circuit potential (OCP) was stabilized in 3.5% NaCl solution. The polarization curves were recorded at a scanning speed of 0.5 mV/s within the range from -250 mV to +250 mV. Electrochemical impedance spectroscopy (EIS) tests were performed on the coating surface of 5 mm in length with an artificially made scratch. In order to study the electrochemical performances of pre-damaged coatings, the frequency ranges of the EIS tests were conducted from 10^{-2} Hz to 10^5 Hz with a

sine wave amplitude of 10 mV and a sample working area of 1 cm^2. During the EIS test, the samples were immersed in a 3.5% NaCl solution for different corrosion durations, and the impedance and corrosion resistance of the coating were evaluated. Three-dimensional corrosion morphology of samples after soaked in 3.5% NaCl solution for 2 weeks was obtained using a laser scanning confocal microscope. Electrical resistance of the coating was tested using an RST-49 four-point probe tester and Agilent 4339B high-precision insulation resistance tester. Each sample was tested three times, and the average value was taken.

4. Results and discussion

4.1. Structure and morphology analysis of modified graphene

To evaluate the crystalline structure of the samples, the as-synthesized GO, Ce^{3+}@rGO and the CeO_2@rGO (12 mM) were studied using XRD and the results are depicted in Fig. 2. As it can be seen in Fig. 2, the peak around 2θ=10.7° (d-spacing 8.3 Å) is attributed to the (001) reflection of GO. Whereas Ce^{3+}@rGO has a peak at 2θ=23°(d-spacing 4.0 Å) belonged to the (002) reflection of rGO, indicating that the reduction of GO occurred during the hydrothermal process. The XRD spectrum of CeO_2@rGO show peaks at 2θ=28.6º，33.1º，47.5º，56.3º corresponding to the (111), (200), (220), (311) crystal planes of CeO_2, respectively, whereas the diffraction peak of rGO disappear. This indicates that after heat treatment, CeO_2 is generated between layers of rGO and its presence disrupts the regular structure of rGO.

【Insert Figure 2】

Fig. 3a and Fig. 3b show the TEM and selected area electron diffraction (SEAD) images of CeO_2@rGO, which was prepared using the Ce^{3+}@rGO (12 mM) after heat treatment in N_2 atmosphere. It can be observed from Fig. 3a that the graphene sheets are relatively smooth and

uniformly attached with nanoparticles on the sheets, and the size of these particles is 5.5±2.6 nm after statistics. The SEAD image in Fig. 3b shows the diffraction patterns of graphene and a series of polycrystal diffraction patterns, which are assigned to those of the cubic cerium oxide (JCPDF No.34-0394).

Fig. 3c and Fig. 3d show the XPS results of the precursor (Ce^{3+}@rGO (12 mM)) and CeO_2@rGO. In the survey spectra shown in Fig. 3c, there are three peaks of C1s, O1s, Ce (Ce3d, Ce4d) for both samples, indicating that the major elements are C, O and Ce. Fig. 3d shows the high-resolution C1s spectra of Ce^{3+}@rGO and CeO_2@rGO, both of which are belonged to the C1s peak of rGO [32]. Compared with that of the Ce^{3+}@rGO, the peak intensity of C-C of CeO_2@rGO is much higher, whereas those of C-O and C=O are much lower. These indicate that the C-O/C=O bonds on the surface of rGO were broken during the heat treatment and the rGO was further reduced. Moreover, the C-C binding energy of Ce^{3+}@rGO does not show much difference with that of the standard rGO (284.60 eV), indicating that Ce^{3+} and rGO are bonded by the electrostatic force [33]. However, the C-C binding energy of CeO_2@rGO is increased, indicating that there is a charge transfer from CeO_2 to rGO. This increases the Fermi energy level of rGO to the conduction band, and the CeO_2 and rGO are covalently bonded [33,34].

【Insert Figure 3】

4.2. Microstructure studies of composite coating

Fig. 4 shows the FT-IR spectra of the prepared epoxy coating, rGO/epoxy coating, and CeO_2@rGO/epoxy coating. The absorption peaks of -OH, C-H, C=O, C=C, C-O, and C-H are observed in all three samples [35]. The main difference is that the rGO/epoxy coating and CeO_2@rGO/epoxy coating have a new absorption peak from aliphatic ether (C-O-C) at 1110

cm^{-1}, which is attributed to the reaction of the hydroxyl groups on the surface of GO, rGO and CeO_2@rGO with the epoxy groups of epoxy resin. In other words, CeO_2@rGO is crosslinked through the covalent bond with the epoxy resin[36]. However, because the CeO_2@rGO has been processed hydrothermally twice, and then calcinated with less oxygen-containing functional groups on its surface compared with that of rGO, the degree of cross-linking and the amplitude of the aliphatic ether peak of CeO_2@rGO/epoxy coatings are much lower than those of the rGO/epoxy coatings.

【Insert Figure 4】

Fig. 5 shows cross-section SEM images (backscattering electron images) of the epoxy coating and CeO_2@rGO/epoxy composite coating, in which the upper part is the coating, and the lower part is the Q235 steel matrix. The layer thickness from the bar coater is ~100 μm after coated twice. Considering the curing rate of coating of 60%, the estimated coating thickness should be about 120 μm. Fig. 5b is a high magnification image of the box area as shown in Fig. 5a. The coating thickness is about 117 μm. There are some pores in the coating caused by evaporation of solvent during curing, and also some white metal particles which were left after mechanical cutting. Fig. 5c shows a cross-section SEM image of the CeO_2@rGO/epoxy composite coating, and Fig. 5d shows the high magnification image of the box area in Fig. 5c. The composite coating thickness is about 111 μm. From both Figs. 5a and 5c, the interface between the coating and the matrix is quite rough, because the steel substrate has been sand-blasted in order to increase its surface roughness and the bonding strength of coating to the substrate.

【Insert Figure 5】

Fig. 6 shows TEM images of CeO_2@rGO/epoxy composite coating with a mass fraction

of CeO_2@rGO of 0.5wt%. The distribution of graphene in epoxy can be clearly revealed due to the different contrast between graphene and substrate. In Fig. 6a, there are black lines (CeO_2@rGO lamella) which are distributed on a grey background of substrate (epoxy). These black lines are distributed uniformly without obvious agglomeration, and they are connected to each other forming a network structure.

In Fig. 6b, there are many fine black particles near these black lines. Fig. 6c is an SEAD image of the box area in Fig. 6b. The diffraction patterns can be assigned to the interplanar crystal spacing of cubic cerium oxides based on the reference of JCPDF No. 34-0394, e.g., (111), (200), (220) and (311) crystal faces of cerium oxide. Fig. 6d shows the STEM image and elemental distributions of the composite coating, and the results confirmed that these particles are ceria. Graphene is evenly dispersed inside the epoxy matrix, and the cerium oxide nanoparticles are distributed uniformly along with the graphene [37].

There are microporous defects in the coating caused by solvent evaporation during coating curing stage (shown by yellow arrows in Fig. 6b), with the size of pores at 50- 200 nm. These defects will affect the corrosion resistance of coating, because the corrosive medium can easily permeate into the matrix along the defects in the coating. As explained in our proposed design mechanism, the CeO_2@rGO nanosheets distributed around these voids can play a physical barrier to prevent the diffusion and penetration of corrosive media and thus effectively delay the corrosion process.

Fig. 6e shows a high-resolution TEM (HR-TEM) image of the interface between CeO_2@rGO and epoxy, and Fig. 6f is an enlarged region in Fig. 6e. Some lattice fringes can be clearly seen in Fig. 6f with distances of 0.31 nm and 0.27 nm, which are corresponding to interplanar spacings of the cerium oxide (111) and (200) planes, respectively. The interplanar

spacing of 0.35 nm is corresponding to the (002) graphene. These results can confirm that the yellow parallel line region in Fig. 6e is CeO_2@rGO, and beyond these regions, the epoxy substrate is dominant. In these figures, the interface layer between epoxy and CeO_2@rGO is dense without any voids. There are two possible reasons for the formation of such dense interfacial layers in the composite coatings. (1) Graphene oxide modified by cerium has a good wettability and is well compatible with epoxy resins; (2) As graphene and epoxy matrix are chemically cross-linked by aliphatic ether, a dense interfacial layer was formed through the strong chemical bonding.

【Insert Figure 6】

4.3. Properties of composite coating

Fig. 7 shows the results of shore hardness of the composite coating with different CeO_2@rGO contents. It can be found that the addition of CeO_2@rGO can improve the hardness of composite coating, and the increase in hardness is proportional to the addition of CeO_2@rGO. Results of FT-IR spectra indicated that graphene oxides were covalently cross-linked with epoxy. These CeO_2@rGO have excellent mechanical properties, which play a critical role of second phase strengthening in the coating. Thus, the hardness of coating has been significantly improved.

【Insert Figure 7】

The organic coating as a good isolating layer protects the metal matrix from corrosive medium. However, during the application, the corrosive solution can permeate into coating gradually along its microporous defects. Therefore, the corrosion medium will permeate into coating gradually and the coating will have different electrochemical characteristics as a function of duration when the coating is immersed inside the corrosive solution. The process

can be divided into the initial stage of immersion, the middle stage of immersion, and the final stage of immersion [38]. Fig. 8 illustrates the equivalent circuit models of the organic coating at different soaking periods in the corrosive conditions. In this figure, R_s, R_t and R_{ct} are solution resistance, coating resistance and charge transfer resistance, respectively, C_c is coating capacitance, C_d is double-layer capacitance and Z_W is Warburg impedance. Z_W means that the electrochemical corrosion of the metal/coating interface is controlled by diffusion, which is the diffusion response of ions or products involved in the corrosion process [23,39].

In the initial stage of immersion, the corrosion solution has not been in contact with the substrate. Therefore, the impedance of coating is mainly controlled by the charge transfer process, and the impedance spectrum has only one time constant. The corresponding physical model can be described by the equivalent circuit shown in Fig. 8a.

With prolonging the immersion time, the corrosion medium reaches the interface between the coating and substrate. The electrochemical reaction occurs at their interfaces, but the coating has not yet shown macroscopic bubbles or holes, which is at the middle stage of immersion. This period is controlled by the charge transfer and diffusion process through the interfaces. The impedance of coating has two different time constants, corresponding to the coating capacitance, and the double-layer capacitor of metal and electrolyte, respectively [38,39]. The corresponding equivalent circuit is shown in Fig. 8b.

When the bubbles and corrosive products are generated on the surface of the coating, the coating has no protective effect to the corrosive medium, which is at the final stage of immersion. For this case, the impedance of the system is mainly determined by the diffusion process of the substrate reaction, and there is no such a time constant of coating capacitance. The corresponding equivalent circuit is shown in Fig. 8c.

【Insert Figure 8】

As explained in the Experimental Section, in order to evaluate the corrosion resistance and failure mechanism of the coating, a 5 mm scratch was artificially created on the coating surface, in order to accelerate the chemical solution's penetration. The EIS analysis of the damaged coating was studied after the different immersion times. Fig. 9 exhibits the EIS Bode diagram of composite coating with different CeO_2@rGO contents after the coating was immersed in 3.5% NaCl solution for different periods of 24 hrs, 72 hrs and 168 hrs. Figs. 9a, 9c and 9e are the double logarithmic impedance-frequency ($|Z|$-f) graphs and Figs. 9b, 9d and 9f are the phase-frequency (θ-f) graphs, respectively. The impedance modulus ($|Z|$) in the low frequency region (below 0.1 Hz) in the $|Z|$-f diagram is independent of frequency and is often used to measure the protective performance of the coating [41]. The impedance modulus at the lowest frequency ($|Z|_{0.01}$) is usually selected. The higher the value of $|Z|_{0.01}$, the better the coating protection performance is. As shown in Figs. 9a and 9b, the impedance of coating shows apparent differences after immersed in the NaCl solution for 24 hrs. In Fig. 9a, the $|Z|_{0.01}$ of CeO_2@rGO/EP-0.50 was maximum and the $|Z|_{0.01}$ of pure epoxy was minimum.

Generally, a peak or valley of the curve corresponds to a time constant in the phase angle Bode diagram of the coating. From Fig. 9b, the EIS results of both the epoxy coating and the CeO_2@rGO/EP-0.50 coating only show one time constant, while the other coatings show two-time constants. The time constants of high frequency and low frequency regions correspond to the coating capacitance and the double-layer capacitance of the metal/electrolyte interface, respectively. Based on the results shown in Figs. 9a and b, after 24-hour immersion, the epoxy coating was already in its late stage of immersion, meaning that the coating has already failed. Whereas the CeO2@rGO/EP-0.50 coating was at its initial stage of immersion, and all the other

coatings were in their middle stage of immersion.

Prolonging the immersion time of coating samples to 72 hrs (Fig. 9c), the values of impedance moduli of all the coatings are decreased. Comparing Figs. 9c and 9d, it can be observed that the epoxy coating and CeO_2@rGO/EP-0.25 coating show only one time constant, while the remaining coatings show two-time constants. Based on this, we can conclude that the CeO_2@rGO/EP-0.25 coating is now at the final stage of immersion, whereas the CeO_2@rGO/EP-0.50 coating is still in the middle stage of immersion with the relatively high value of impedance modulus.

The results obtained from the coating after immersion for 168 hrs are shown in Fig. 9f. Only the CeO_2@rGO/EP-0.50 and CeO_2@rGO/EP-0.75 coatings show characteristics with two-time constants, whereas the CeO_2@rGO/EP-1.00 coating only shows one-time constant, indicating that this coating reaches its late stage of immersion. In general, the corrosion medium would diffuse quickly into the epoxy coating through the scratches in the immersion process, and the coating failed after immersion for 24 hrs. While for the composite coatings, the presence of CeO_2@rGO would greatly delay this process.

【Insert Figure 9】

In order to have a better understanding of the corrosion behavior of electrolyte to coated metal, the equivalent circuits corresponding to the results in different immersion stages shown in Fig. 9 were fitted using the Zview software according to the characteristics of impedance spectra for each coating. In the equivalent circuit, the measured value of the coating capacitance is deviated from the ideal value due to the inhomogeneity or high roughness of the coating surface. A constant phase element (CPE) is used to replace the coating capacitance which has the deviation from the ideal capacitance [42]. The fitted electrochemical parameters are

summarized in Table 2. R_c is the resistance of coating, which usually reflects the effectiveness of the coating at the initial stage of immersion. R_{ct} is the charge transfer resistance, which reflects the reaction rate of coated metal in the middle-late stage of immersion. A higher R_{ct} value indicates a lower coating corrosion rate. Thus, the value of R_t=R_c+R_{ct} can be used to reflect the protective effect of the coating during the whole immersion process [43]. The coating capacitance C_c is related to the water-proof properties of the coating. Since the electrolyte solution has a large value of permittivity, it will significantly enhance the coating's capacitance when the electrolyte solution permeates into the coating. According to Burg's Equation [44], the value of C_c can be obtained from the corresponding CPE parameters, and the conversion equation is shown in Eq. (5):

$$C_c = (Y_0 R_c^{1-n})^{\frac{1}{n}} \quad (5)$$

where C_c is the coating capacitance, R_c is the coating resistance, Y_0 is the coating admittance, n is an empirical constant with range of $0 \leq n \leq 1$.

Fig. 10 depicts the changes of coating's C_c and R_t values with immersion time based on the equivalent circuit parameters listed in Table 2. In Fig. 10a, the C_c value of the epoxy coating is the largest and does not change much with time, indicating that the electrolyte has been completely permeated into the epoxy after 24 hrs. The composite coating with CeO_2@rGO content of 0.25~0.75wt.% exhibits a small C_c value after 24 hrs, attributed to that the CeO_2@rGO nanosheets are uniformly distributed in the composite coating which could effectively prevent the electrolyte infiltration. With the further extension of immersion time, the electrolyte solution in the coating becomes gradually saturated, and coating shows a similar C_c value. However, the C_c value of the composite coating is similar to that of the epoxy coating when the content of CeO_2@rGO reaches 1.0 wt.%. This is because the agglomeration of large

content of graphene will weaken the effective shielding effect, and result in more defects in the coating. Among all the coatings, the sample of CeO_2@rGO/EP-0.50 has the minimum coating capacitance during the whole soaking time, indicating the optimum value is 0.5wt.% rare-earth modified graphene to the waterborne epoxy coating. Fig. 10b shows the changes of R_t value as a function of coating soaking time. From this figure, the changing trends of the R_t value of each coating is similar to that of C_c value. The R_t values are decreased with the immersion time, and the CeO_2@rGO/EP-0.50 coating has the largest R_t value.

【Insert Figure 10】

【Insert Table 2】

Tafel polarization curve is a standard method for studying the corrosion behavior of metals, and the corrosion resistance of coating can be characterized by self-corrosion potential (E_{corr}), self-corrosion current density (I_{corr}), corrosion rate (v_{corr}) and protective efficiency (P_i). Self-corrosion potential is associated to the difficulty of corrosion, and self-corrosion current density is related to the rate of corrosion. The higher value of E_{corr} and the lower value of I_{corr} for the coating indicate a better corrosion resistance of the coating [45]. The corrosion rate (v_{corr}) and protection efficiency (P_i) of the coating can be obtained from Eqs. (6) and (7), respectively [28].

$$v_{corr} = \frac{87600 E_w I_{corr}}{n \rho F} \tag{6}$$

$$P_i = \left(1 - \frac{I_{corr}}{I_{corr}^S}\right) \times 100\% \tag{7}$$

In Eq. (6), I_{corr} can be obtained by linear fitting of polarization curve, E_w is the molecular weight (55.85 g/mol) of substrate steel, ρ is the density (7.85 g/cm^2) of substrate steel, n is the valence of iron ions, and F is the Faraday constant (26.8 A·h/mol). In Eq. (7), I^S_{corr} is the self-corrosion current density of substrate steel.

Fig. 11 shows the polarization analysis results of both steel and the coated steel. Using the Cview software, the obtained parameters were obtained and the results are listed in Table 3. The Tafel polarization curves of epoxy coating and composite coatings with different CeO_2@rGO contents are shown in Fig. 11a. The obtained E_{corr} and I_{corr} values of the epoxy coating are -0.642 V and 2.239 μA/cm^2, respectively. However, after adding the different contents of CeO_2@rGO into the epoxy coating, the E_{corr} value of composite coating is increased and the I_{corr} value is decreased expect for the CeO_2@rGO/EP-1.00 coating. The high I_{corr} value of CeO_2@rGO/EP-1.00 coating is due to the good electric conductivity of graphene and the high graphene content could form a seepage network in coating, which will increase the conductivity and I_{corr} of the coating.

In general, the CeO_2@rGO as a filler can enhance the corrosion resistance of epoxy coating. With the increase of CeO_2@rGO fillers, the corrosion resistance of composite coating is increased firstly but then decreased. When the content of CeO_2@rGO was 0.50 wt.%, the E_{corr} value of composite coating was increased by 0.121 V and I_{corr} value was decreased by 14.35 times compared with the epoxy coating, and the corrosion rate was reduced from 0.025 mm/year to 0.002 mm/year. This is consistent with the EIS test results that the CeO_2@rGO/EP-0.50 coating shows the best corrosion resistance.

The polarization curves of Q235 steel, rGO/EP-0.50 coating and CeO_2@rGO/EP-0.50 coating are shown in Fig. 11b. Comparing the corrosion resistance of rGO/EP-0.5 coating and CeO_2@rGO/EP-0.50 coating, the E_{corr} value of CeO_2@rGO/EP-0.50 coating was increased by 0.100 V and the I_{corr} value was decreased by 8.65 times compared with those of the rGO/EP-0.50 coating. Therefore, the CeO_2@rGO/EP-0.50 sample has a better protection efficiency.

【Insert Figure 11】

【Insert Table 3】

In order to better understand the changes of corrosion characteristics of the coating, the three-dimension contour morphology of the coating after immersion in 3.5% NaCl solution for 14 days was observed using a laser scanning confocal microscope, and the images aere shown in Fig. 12. In this image, different colors represent different heights, with red being the highest, yellow the second, then green, and blue the lowest. It can be observed that the surface morphology of each coating has different characteristics after it was immersed in NaCl solution for 14 days. Fig. 12a is the surface morphology of the epoxy coating, and there are many bubbles on the surface, which is due to the corrosion of the metal substrate under the coating and the accumulation of corrosion products. The CeO_2@rGO/EP-0.25 coating and CeO_2@rGO/EP-0.75 coating show blistering morphologies as shown in Figs. 12b and 12e. While the surface of CeO_2@rGO/EP-0.50 coating is smoother than that of the EP. The CeO_2@rGO/EP-0.25 and CeO_2@rGO/EP-0.75 coatings show no obvious blistering, but only some bubbles with a much smaller size. This explains that the CeO_2@rGO/EP-0.50 coating shows less corrosive pitting on the substrate and a better protection performance. From Fig. 12f, even though the CeO_2@rGO/EP-1.00 coating does not show any blistering, there are many holes observed, which indicates that the coating has been perforated after soaked for 14 days. In conclusion, after soaking the coated samples in NaCl solution for 14 days, the degree of coating failure is quite different and the CeO_2@rGO/EP-0.50 coating shows the best performance.

【Insert Figure 12】

According to Eq. (8), the mass fraction of rare-earth modified graphene was converted into volume fraction, and the relationship between conductivity and packing volume fraction of

CeO_2@rGO filled epoxy resin composite coating was obtained. The results are shown in Fig. 13. From this figure, the electrical conductivity of the composite coating shows a typical percolation phenomenon [46,47]. The conductivity of the composite coating increases slightly with the volume fraction of filler when the content of CeO_2@rGO is lower than 0.10 vol.%. The CeO_2@rGO/EP coating exhibits a transition from insulator to semiconductor when the content of CeO_2@rGO is increased from 0.1 vol.% to 0.3 vol.%. The conductivity of the composite coating reaches a value of 10^{-2} S/m when the content of CeO_2@rGO exceeds 0.4 vol.%, and the conductivity of coting is significantly improved by nine orders of magnitude compared with that of the epoxy coating. When the CeO_2@rGO content is 0.5 wt.% (about 0.25vol. %), the conductivity of the composite coating is in the order of 10^{-5} S/m, which is good enough to be used as an antistatic material [7,48].

$$V_f = \frac{\omega_f}{\omega_f + (\rho_f/\rho_m)(1-\omega_f)} \tag{8}$$

where ω_f is the mass fraction of CeO_2@rGO, ρ_f is the density of CeO_2@rGO, which is estimated to be about 2.6 g/cm^2, ρ_m is the density of epoxy, e.g., 1.2 g/cm^2.

【Insert Figure13】

According to the theory of percolation threshold [47], with the increase of the content of conductive filler, the conductivity of polymer will be dramatically increased at a critical point. At this critical content, the filler can form a conductive network in the substrate to improve the conductivity property of the composite. The percolation threshold of composite coating can be estimated by the Eq. (9) [49].

$$\sigma_c = \sigma_{gr}\left[\frac{(V_f - V_c)}{(1-V_c)}\right]^t \quad V_f > V_c \tag{9}$$

where V_f is the volume fraction of CeO_2@rGO, V_c is the volume fraction of penetration threshold, σ_c and σ_{gr} are the conductivity values of composite coating and CeO_2@rGO,

respectively, t is the 'universal critical exponent'. As shown in Fig. 14, the double logarithmic diagram of σ_c and V_f-V_c shows the optimal fitting results of V_c= 0.231 vol.% and t = 1.45. The penetration threshold obtained in this study is far lower than the reported threshold of graphene/epoxy composite [36,47], which proves that modification of CeO_2 nanoparticles on the graphene surface can improve its dispersion in the composite coating.

After addition of CeO_2@rGO, the E_{corr} value of composite coating is increased and the I_{corr} value is reduced except for the CeO_2@rGO/EP-1.00 coating. The CeO_2@rGO-0.50 composite coating shows the best protective effect. When the content of CeO_2@rGO reaches 1.00 wt.%, the graphene forms a percolation network in the coating, which results in an enhanced conductivity and an increased I_{corr} value. From the EIS results, the presence of CeO_2@rGO results in a longer protection time for the composite coating. After soaked for 168 hours, only the CeO_2@rGO-0.50 and CeO_2@rGO-0.75 coatings still have protective effect, whereas the CeO_2@rGO-1.00 coating totally fails. These results are consistent with the proposed coating protection mechanism. Graphene can improve the protective property of the coating, but a large content of graphene can accelerate corrosion. As we know cerium can inhibit galvanic corrosion caused by graphene, but its effect is limited. Thus, the corrosion resistance of CeO_2@rGO-1.00 coating is poor.

5. Conclusion

In this work, we proposed a new protective mechanism of coating and prepared CeO_2@rGO as a filler to improve the corrosion resistance and electrical properties of epoxy coatings. The results showed that CeO_2 particles were uniformly distributed on the surface of graphene and covalently bonded. The CeO_2@rGO nanoparticles were homogeneously

dispersed in the epoxy matrix, forming a dense interface layer crosslinked by aliphatic ether bonds. Moreover, when the content of modified graphene was 0.45 vol.%, the conductivity of the composite coating was increased by nine orders of magnitude to a maximum value of 2.28 × 10^{-2} S/m with a low permeability threshold of 0.231 vol.%. In addition, the content of CeO_2@rGO also affected the corrosion resistance of the coating and the experimental results were consistent with proposed coating protection mechanism. High content of graphene accelerated corrosion and ceriuminhibited galvanic corrosion caused by graphene, but its effect was limited. The composite coating had the best corrosion resistance/antistatic comprehensive performance when the content of CeO_2@rGO was 0.50 wt.%. The E_{corr} of composite coating was increased by 0.121 V and I_{corr} was decreased by 14.35 times compared with those of the epoxy coating. The corrosion rates were reduced from 0.025 mm/year to 0.002 mm/year and the electrical conductivity reached the antistatic level of 10^{-5} S/m.

Acknowledgement

The authors would like to acknowledge the financial supports from Shaanxi Coal Industry Group United Fund of China (No.2019JLM-2), Xi'an Science research project of China (No.2020KJRC0089) and Electrical Materials and Infiltration Key Laboratory of Shaanxi Province Projects (No.17JS080), Newton Mobility Grant (IE161019) through Royal Society.

References

[1] W. Ke, Progress in public inquiry concerning corrosion in chinese industrial and natural environments, Corros. Prot. 25 (2004) 1–8. https://doi.org/10.3969/j.issn.1005-748X.2004.01.001.

[2] H. Wei, J. Xia, W. Zhou, L. Zhou, G. Hussain, Q. Li, K. (Ken) Ostrikov, Adhesion and

cohesion of epoxy-based industrial composite coatings, Compos. Part B Eng. 193 (2020) 108035. https://doi.org/10.1016/j.compositesb.2020.108035.

[3] M. Liu, X. Mao, H. Zhu, A. Lin, D. Wang, Water and corrosion resistance of epoxy-acrylic-amine waterborne coatings: Effects of resin molecular weight, polar group and hydrophobic segment, Corros. Sci. 75 (2013) 106–113. https://doi.org/10.1016/j.corsci.2013.05.020.

[4] Y. Qu, The present situation and developing direction of heavy-duty coating at home and abroad, Chem. Ind. 31 (2013) 25–34. https://doi.org/10.3969/j.issn.1673-9647.2013.08.004.

[5] E. Han, J. Chen, Y. Su, M. Liu, Corrosion protection techniques of marine engineering structure and ship equipment-current status and future trend, Mater. China. 33 (2014) 65–76. https://doi.org/10.7502/j.issn.1674-3962.2014.02.01.

[6] M. Sangermano, D. Foix, G. Kortaberria, M. Messori, Multifunctional antistatic and scratch resistant UV-cured acrylic coatings, Prog. Org. Coatings. 76 (2013) 1191–1196. https://doi.org/10.1016/j.porgcoat.2013.03.030.

[7] A. Zhu, H. Wang, S. Sun, C. Zhang, The synthesis and antistatic, anticorrosive properties of polyaniline composite coating, Prog. Org. Coatings. 122 (2018) 270–279. https://doi.org/10.1016/j.porgcoat.2018.06.004.

[8] Y. Liu, X. Jian, X. Su, F. Luo, J. Xu, J. Wang, X. He, Y. Qu, Electromagnetic interference shielding and absorption properties of Ti3SiC2/nano Cu/epoxy resin coating, J. Alloys Compd. 740 (2018) 68–76. https://doi.org/10.1016/j.jallcom.2018.01.017.

[9] L.-C. Jia, C.-G. Zhou, W.-J. Sun, L. Xu, D.-X. Yan, Z.-M. Li, Water-based conductive

ink for highly efficient electromagnetic interference shielding coating, Chem. Eng. J. 384 (2020) 123368. https://doi.org/10.1016/j.cej.2019.123368.

[10] F. Chi, Y. Zeng, C. Liu, N. Pan, C. Ding, F. Yi, Highly stable self-cleaning antireflection coatings from fluoropolymer brush grafted silica nanoparticles, Appl. Surf. Sci. 507 (2020) 144836. https://doi.org/10.1016/j.apsusc.2019.144836.

[11] W. Shen, L. Feng, X. Liu, H. Luo, Z. Liu, P. Tong, W. Zhang, Multiwall carbon nanotubes-reinforced epoxy hybrid coatings with high electrical conductivity and corrosion resistance prepared via electrostatic spraying, Prog. Org. Coatings. 90 (2016) 139–146. https://doi.org/10.1016/j.porgcoat.2015.10.006.

[12] A. Ghasemi-Kahrizsangi, H. Shariatpanahi, J. Neshati, E. Akbarinezhad, Corrosion behavior of modified nano carbon black/epoxy coating in accelerated conditions, Appl. Surf. Sci. 331 (2015) 115–126. https://doi.org/10.1016/j.apsusc.2015.01.038.

[13] T. Wang, H. Ge, K. Zhang, A novel core-shell silica@graphene straticulate structured antistatic anticorrosion composite coating, J. Alloys Compd. 745 (2018) 705–715. https://doi.org/10.1016/j.jallcom.2018.02.222.

[14] B. Zhang, J. Wang, T. Wang, X. Su, S. Yang, W. Chen, J. Wang, J. Sun, J. Peng, High-performance microwave absorption epoxy composites filled with hollow nickel nanoparticles modified graphene via chemical etching method, Compos. Sci. Technol. 176 (2019) 54–63. https://doi.org/10.1016/j.compscitech.2019.04.001.

[15] A.K. Geim, K.S. Novoselov, The rise of graphene, Nat. Mater. 6 (2007) 183–191. https://doi.org/10.1038/nmat1849.

[16] C. Lee, X. Wei, J. Kysar, J. Hone, Measurement of the Elastic Properties and Intrinsic Strength of Monolayer Graphene, Science. 321 (2008) 385–388.

https://doi.org/10.1126/science.1157996.

[17] M. Gagné, D. Therriault, Lightning strike protection of composites, Prog. Aerosp. Sci. 64 (2014) 1–16. https://doi.org/10.1016/j.paerosci.2013.07.002.

[18] A.A. Balandin, S. Ghosh, W. Bao, I. Calizo, D. Teweldebrhan, F. Miao, C.N. Lau, Superior Thermal Conductivity of Single-Layer Graphene, Nano Lett. 8 (2008) 902–907. https://doi.org/10.1021/nl0731872.

[19] H.K. Chae, D.Y. Siberio-Pérez, J. Kim, Y. Go, M. Eddaoudi, A.J. Matzger, M. O'Keeffe, O.M. Yaghi, M.D. and D. Group, A route to high surface area, porosity and inclusion of large molecules in crystals, Nature. 427 (2004) 523–527. https://doi.org/10.1038/nature02311.

[20] X. Zhao, K. Li, W. Li, Y. Zhao, H. Liu, Study on the corrosion protection mechanismof graphene modified anticorrosive coatings, China Coatings. 32 (2017) 18–23. https://doi.org/10.13531/j.cnki.china.coatings.2017.02.005.

[21] M. Yang, B. Liu, J. Xia, Y. Liu, Z. Shi, X. Lv, Study on the properties of a novel electrostatic conductive and anti-corrosive composite coating improved by graphene nanosheets, Prog. Org. Coatings. 136 (2019) 105244. https://doi.org/10.1016/j.porgcoat.2019.105244.

[22] K.-C. Chang, M.-H. Hsu, H.-I. Lu, M.-C. Lai, P.-J. Liu, C.-H. Hsu, W.-F. Ji, T.-L. Chuang, Y. Wei, J.-M. Yeh, W.-R. Liu, Room-temperature cured hydrophobic epoxy/graphene composites as corrosion inhibitor for cold-rolled steel, Carbon N. Y. 66 (2014) 144–153. https://doi.org/10.1016/j.carbon.2013.08.052.

[23] S. Pourhashem, M.R. Vaezi, A. Rashidi, Investigating the effect of SiO2-graphene oxide hybrid as inorganic nanofiller on corrosion protection properties of epoxy

coatings, Surf. Coatings Technol. 311 (2017) 282–294. https://doi.org/10.1016/j.surfcoat.2017.01.013.

[24] B. Ramezanzadeh, A. Ahmadi, M. Mahdavian, Enhancement of the corrosion protection performance and cathodic delamination resistance of epoxy coating through treatment of steel substrate by a novel nanometric sol-gel based silane composite film filled with functionalized graphene oxide nanosheets, Corros. Sci. 109 (2016) 182–205. https://doi.org/10.1016/j.corsci.2016.04.004.

[25] X. Jiang, Z. Zhu, Y. Zhou, C. Shi, Preparation and Characterization of rGO -PPD - MWCNT Hybrid Nano -Composites for Modifying Conductive Coatings, Mater. Prot. 52 (2019) 20–26. https://doi.org/10.16577/j.cnki.42-1215/tb.2019.06.004.

[26] Y. Zhan, J. Zhang, X. Wan, Z. Long, S. He, Y. He, Epoxy composites coating with Fe3O4 decorated graphene oxide: Modified bio-inspired surface chemistry, synergistic effect and improved anti-corrosion performance, Appl. Surf. Sci. 436 (2018) 756–767. https://doi.org/10.1016/j.apsusc.2017.12.095.

[27] Y. Wang, Y. Li, J. Zhu, Y. Zhao, H. Li, Surface modification mechanism graphene oxide by adding rare earth, J. Mater. Eng. 46 (2018) 29–35. https://doi.org/10.11868/j.issn.1001-4381.2017.000429.

[28] S. Qiu, W. Li, W. Zheng, H. Zhao, L. Wang, Synergistic Effect of Polypyrrole-Intercalated Graphene for Enhanced Corrosion Protection of Aqueous Coating in 3.5% NaCl Solution, ACS Appl. Mater. Interfaces. 9 (2017) 34294–34304. https://doi.org/10.1021/acsami.7b08325.

[29] M. Motamedi, M. Ramezanzadeh, B. Ramezanzadeh, M. Mahdavian, One-pot synthesis and construction of a high performance metal-organic structured nano

pigment based on nanoceria decorated cerium (III)-imidazole network (NC/CIN) for effective epoxy composite coating anti-corrosion and thermo-mechanical properties impro, Chem. Eng. J. 382 (2020) 122820. https://doi.org/10.1016/j.cej.2019.122820.

[30] N.N. Taheri, B. Ramezanzadeh, M. Mahdavian, G. Bahlakeh, In-situ synthesis of Zn doped polyaniline on graphene oxide for inhibition of mild steel corrosion in 3.5wt.% chloride solution, J. Ind. Eng. Chem. 63 (2018) 322–339. https://doi.org/10.1016/j.jiec.2018.02.033.

[31] B. Ramezanzadeh, G. Bahlakeh, M. Ramezanzadeh, Polyaniline-cerium oxide (PAni-CeO2) coated graphene oxide for enhancement of epoxy coating corrosion protection performance on mild steel, Corros. Sci. 137 (2018) 111–126. https://doi.org/10.1016/j.corsci.2018.03.038.

[32] S. Stankovich, D.A. Dikin, R.D. Piner, K.A. Kohlhaas, A. Kleinhammes, Y. Jia, Y. Wu, S.B.T. Nguyen, R.S. Ruoff, Synthesis of graphene-based nanosheets via chemical reduction of exfoliated graphite oxide, Carbon N. Y. 45 (2007) 1558–1565. https://doi.org/10.1016/j.carbon.2007.02.034.

[33] D. Joung, V. Singh, S. Park, A. Schulte, S. Seal, S.I. Khondaker, Anchoring ceria nanoparticles on reduced graphene oxide and their electronic transport properties, J. Phys. Chem. C. 115 (2011) 24494–24500. https://doi.org/10.1021/jp206485v.

[34] M. Vanitha, Keerthi, P. Cao, N. Balasubramanian, Ag nanocrystals anchored CeO2/graphene nanocomposite for enhanced supercapacitor applications, J. Alloys Compd. 644 (2015) 534–544. https://doi.org/10.1016/j.jallcom.2015.03.221.

[35] F. Contu, L. Fenzy, S.R. Taylor, An FT-IR investigation of epoxy coatings as a function of electrolyte composition, Prog. Org. Coatings. 75 (2012) 92–96.

https://doi.org/10.1016/j.porgcoat.2012.04.001.

[36] W. Zheng, W.G. Chen, Q. Zhao, S.X. Ren, Y.Q. Fu, Interfacial structures and mechanisms for strengthening and enhanced conductivity of graphene/epoxy nanocomposites, Polymer (Guildf). 163 (2019) 171–177. https://doi.org/10.1016/j.polymer.2018.12.055.

[37] W. Zheng, W.G. Chen, T. Feng, W.Q. Li, X.T. Liu, L.L. Dong, Y.Q. Fu, Enhancing chloride ion penetration resistance into concrete by using graphene oxide reinforced waterborne epoxy coating, Prog. Org. Coatings. 138 (2020). https://doi.org/10.1016/j.porgcoat.2019.105389.

[38] C. Cao, J. Zhang, An introduction to electrochemical impedance spectroscopy, Beijing, 2002.

[39] M. Cui, S. Ren, J. Pu, Y. Wang, H. Zhao, L. Wang, Poly(o-phenylenediamine) modified graphene toward the reinforcement in corrosion protection of epoxy coatings, Corros. Sci. 159 (2019) 108131. https://doi.org/10.1016/j.corsci.2019.108131.

[40] J. Ding, O. ur Rahman, W. Peng, H. Dou, H. Yu, A novel hydroxyl epoxy phosphate monomer enhancing the anticorrosive performance of waterborne Graphene/Epoxy coatings, Appl. Surf. Sci. 427 (2018) 981–991. https://doi.org/10.1016/j.apsusc.2017.08.224.

[41] M. Conradi, A. Kocijan, D. Kek-Merl, M. Zorko, I. Verpoest, Mechanical and anticorrosion properties of nanosilica-filled epoxy-resin composite coatings, Appl. Surf. Sci. 292 (2014) 432–437. https://doi.org/10.1016/j.apsusc.2013.11.155.

[42] P. Córdoba-Torres, T.J. Mesquita, O. Devos, B. Tribollet, V. Roche, R.P. Nogueira, On the intrinsic coupling between constant-phase element parameters α and Q in

electrochemical impedance spectroscopy, Electrochim. Acta. 72 (2012) 172–178. https://doi.org/10.1016/j.electacta.2012.04.020.

[43] N. Parhizkar, B. Ramezanzadeh, T. Shahrabi, Corrosion protection and adhesion properties of the epoxy coating applied on the steel substrate pre-treated by a sol-gel based silane coating filled with amino and isocyanate silane functionalized graphene oxide nanosheets, Appl. Surf. Sci. 439 (2018) 45–59. https://doi.org/10.1016/j.apsusc.2017.12.240.

[44] B. Hirschorn, M.E. Orazem, B. Tribollet, V. Vivier, I. Frateur, M. Musiani, Determination of effective capacitance and film thickness from constant-phase-element parameters, Electrochim. Acta. 55 (2010) 6218–6227. https://doi.org/10.1016/j.electacta.2009.10.065.

[45] Y.-T. Lin, T.-M. Don, C.-J. Wong, F.-C. Meng, Y.-J. Lin, S.-Y. Lee, C.-F. Lee, W.-Y. Chiu, Improvement of mechanical properties and anticorrosion performance of epoxy coatings by the introduction of polyaniline/graphene composite, Surf. Coatings Technol. 374 (2019) 1128–1138. https://doi.org/10.1016/j.surfcoat.2018.01.050.

[46] T. Tang, D. He, The study on conductive percolation behavior of CB/CNTs/EP composites, Carbon Tech. 35 (2016) 7–10. https://doi.org/10.14078/j.cnki.1001-3741.2016.01.002.

[47] A.J. Marsden, D.G. Papageorgiou, C. Vallés, A. Liscio, V. Palermo, M.A. Bissett, R.J. Young, I.A. Kinloch, Electrical percolation in graphene-polymer composites, 2D Mater. 5 (2018) aac055. https://doi.org/10.1088/2053-1583/aac055.

[48] H.-B. Zhang, Q. Yan, W.-G. Zheng, Z. He, Z.-Z. Yu, Tough Graphene−Polymer Microcellular Foams for Electromagnetic Interference Shielding, ACS Appl. Mater.

Interfaces. 3 (2011) 918–924. https://doi.org/10.1021/am200021v.

[49] S. Stankovich, D. Dikin, G. Dommett, K. Kohlhaas, E. Zimney, E. Stach, R. Piner, S. Nguyen, R. Ruoff, Graphene-Based Composite Materials, Nature. 442 (2006) 282–286. https://doi.org/10.1038/nature04969.

Tables

Table1 Chemical elements of substrate Q235 steel.

Component	C	Mn	Si	P	Si	Fe
Content (wt.%)	0.220	0.480	0.05	0.022	0.012	residue

Table 2 The electrochemical parameters extracted from the EIS data of coating.

Sample	Time(hour)	Equivalent circuit	R_c ($\Omega \cdot cm^2$)	CPE_c		R_{ct} ($\Omega \cdot cm^2$)
				Y_0($n\Omega^{-1} \cdot cm^{-2} \cdot s^{-n}$)	n	
Neat Epoxy	24	$R_s(C_c(R_c(C_d(R_{ct}W_s)))$	71.53	672	0.752	1562
	72		27.23	955	0.731	1211
	168		16.24	1373	0.714	949.9
CeO_2@rGO/EP-0.25	24	$R_s(C_c(R_c(C_dR_{ct})))$	951.8	111	0.694	3733
	72	$R_s(C_c(R_c(C_d(R_{ct}W_s)))$	300.8	853	0.619	1746
	168		79.07	1765	0.620	1672
CeO_2@rGO/EP-0.50	24	$R_s(R_cC_c)$	352100	9.26	0.894	/
	72	$R_s(C_c(R_c(C_dR_{ct})))$	800.2	118	0.814	74897
	168		586.3	800	0.728	41006
CeO_2@rGO/EP-0.75	24	$R_s(C_c(R_c(C_dR_{ct})))$	185	466	0.774	9646
	72		138.1	839	0.728	6195
	168		154.2	795	0.687	3094
CeO_2@rGO/EP-1.00	24	$R_s(C_c(R_c(C_dR_{ct})))$	890.2	482	0.733	1559
	72		645.4	628	0.599	1435.9
	168	$R_s(C_c(R_c(C_d(R_{ct}W_s)))$	236	1193	0.664	864.7

Table 3 Polarization curve test results for Q235 steel and CeO_2@rGO/epoxy composite coatings.

Sample	E_{corr}(V)	I_{corr}(μA/cm^2)	v_{corr}(mm/year)	P_i (%)
Q235 steel	−0.829	46.774	0.54387	/
Neat Epoxy	−0.642	2.239	0.02603	95.21315
CeO_2@rGO/EP-0.25	−0.572	0.380	0.00442	99.18758
CeO_2@rGO/EP-0.50	−0.521	0.156	0.00181	99.66648
CeO_2@rGO/EP-0.75	−0.630	0.851	0.00991	98.18061
CeO_2@rGO/EP-1.00	−0.601	3.090	0.03593	93.39377
rGO/EP-0.50	−0.621	1.349	0.01569	97.11592

Figure captions

Fig.1. Illustrations of protective mechanism of (a) pure epoxy coating and (b) CeO_2@rGO/epoxy nanocomposite coating.

Fig.2. XRD patterns of (a)GO, Ce^{3+}@rGO and (b)CeO_2@rGO prepared with different concentration of cerium chloride.

Fig.3. Microstructures of CeO_2@rGO(12mM). (a) TEM image, (b) SEAD pattern, (c) XPS survey spectra and (d) high-resolution C1s spectrum of Ce^{3+}@rGO (12mM) and CeO_2@rGO (12mM).

Fig. 4. FT-IR spectra of the neat epoxy coating, graphene/epoxy nanocomposite coating and rare earth modified graphene /epoxy nanocomposite coating.

Fig. 5. SEM images of Cross-section of epoxy coating and nanocomposite coatings: (a) epoxy coating, (b) high magnification images of the box position in (a), (c) CeO_2@rGO nanocomposites coatings, (d) high magnification images of the box position in (c).

Fig. 6. TEM images of rare earth modified graphene/epoxy nanocomposite coating. (a) to (b): the low magnification images, (c) the SEAD pattern of the box position in (b), (d) STEM-EDS image of nanocomposite coating, (e) and (f):HR-TEM of interfacial region between graphene and epoxy.

Fig. 7. Shore hardness values of nanocomposite coatings with different CeO_2@rGO contents.

Fig. 8. The equivalent circuit diagrams of composite coatings in different immersion periods, (a) initial immersion, (b) middle stage of immersion, (c) final stage of immersion [39,40].

Fig. 9. Bode diagram of EP and CeO_2@rGO/epoxy nanocomposite coatings during 168 hrs immersion in 3.5% NaCl solution. (a), (c) and (e) is the impedance versus frequency of each coating for 24 hrs, 72 hrs, 168 hrs； (b), (d) and (f) is the phase change of the coatings with

frequency for 24 hrs, 72 hrs, 168 hrs.

Fig. 10. Time-dependent variation of the electrical parameters (a) C_c and (b) R_t derived from fitting data for Neat epoxy and CeO_2@rGO/EP composite during immersion.

Fig. 11. (a) Tafel polarization curves of Neat Epoxy and different CeO_2@rGO/EP contents, (b) Tafel polarization curves for Q235 steel, rGO/EP-0.50, CeO_2@rGO/epoxy composite coatings.

Fig.12. 3D Reconstruction images of epoxy coating and modified graphene/epoxy nanocomposite coating grafter immersion in 3.5% NaCl solution for 14 days. (a) Neat Epoxy (b) CeO_2@rGO/EP-0.25, (c) CeO_2@rGO/EP-0.50, (d) high magnification of CeO_2@rGO/EP-0.50, (e) CeO_2@rGO/EP-0.75, (f) CeO_2@rGO/EP-1.00.

Fig.13. The electrical conductivity versus conductive filler content for CeO_2@rGO/epoxy nanocomposite coatings. The inset shows a double-logarithmic plot of electrical conductivity.

Figures:

The figures attached at the end of the manuscript may not be clear, we have provided separate uploaded figures file.

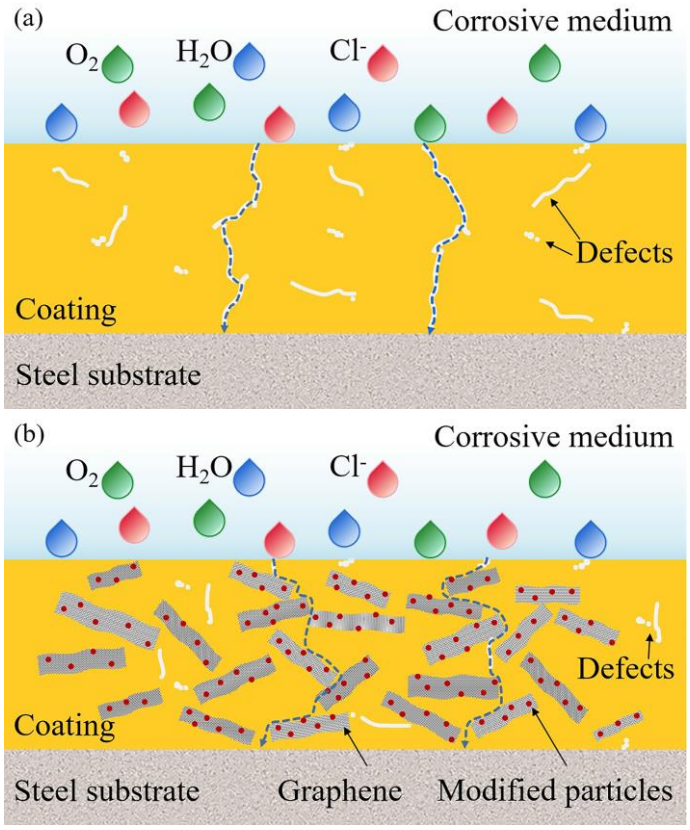

Fig. 1.

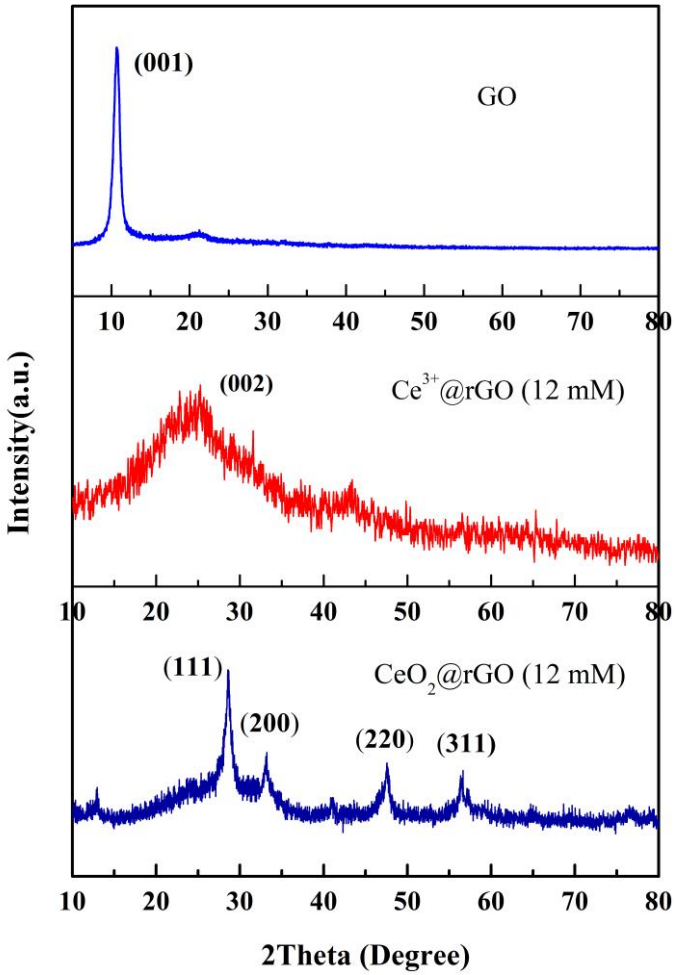
(001)
GO
10
20
30
40
50
60
70
80
(002)
Ce3+@rGO (12 mM)
Intensity(a.u.)
(111)
(200)
(220)
(311)
CeO2@rGO (12 mM)
2Theta (Degree)

Fig. 2.

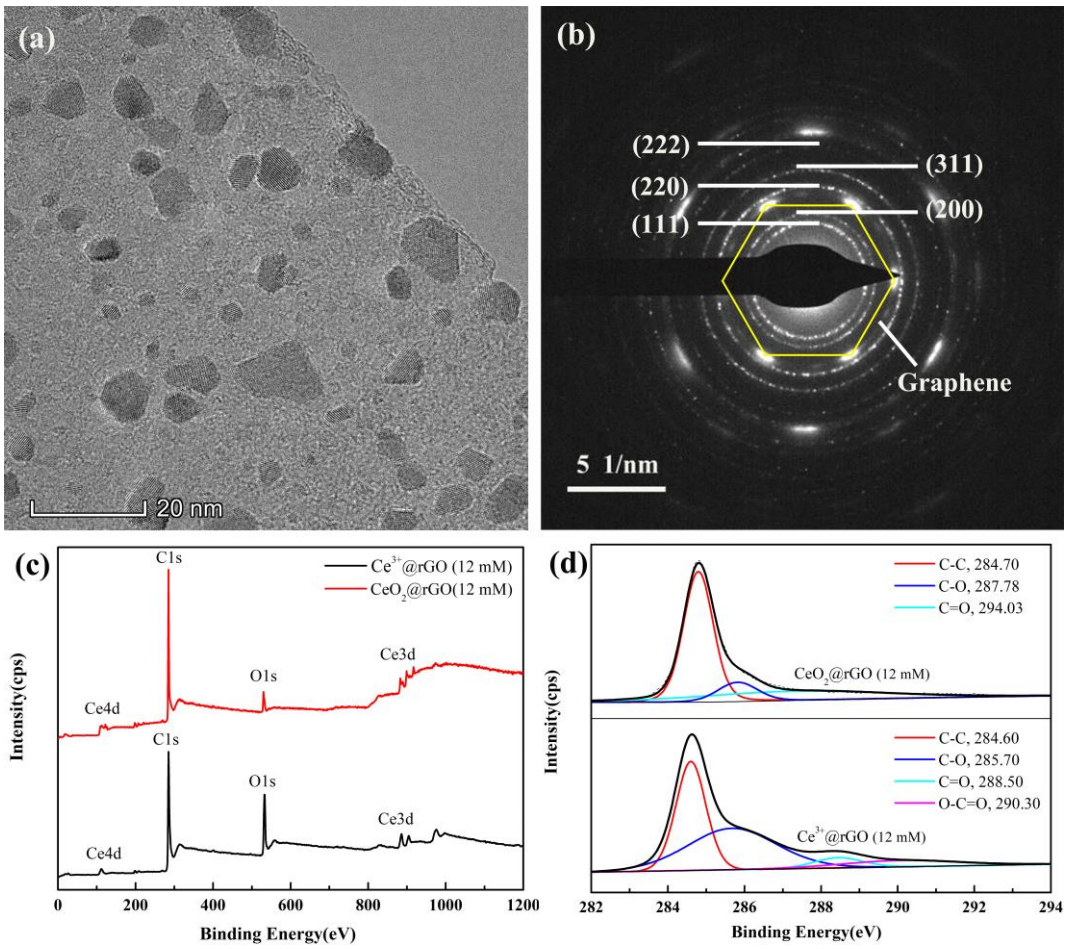
(a)
20 nm
(b)
(222)
(311)
(220)
(200)
(111)
Graphene
5 1/nm
(c)
C1s
Ce3+@rGO (12 mM)
CeO2@rGO(12 mM)
Ce3d
O1s
Ce4d
Intensity(cps)
Binding Energy(eV)
(d)
C-C, 284.70
C-O, 287.78
C=O, 294.03
CeO2@rGO (12 mM)
C-C, 284.60
C-O, 285.70
C=O, 288.50
O-C=O, 290.30
Ce3+@rGO (12 mM)
Intensity(cps)
Binding Energy(eV)

Fig. 3.

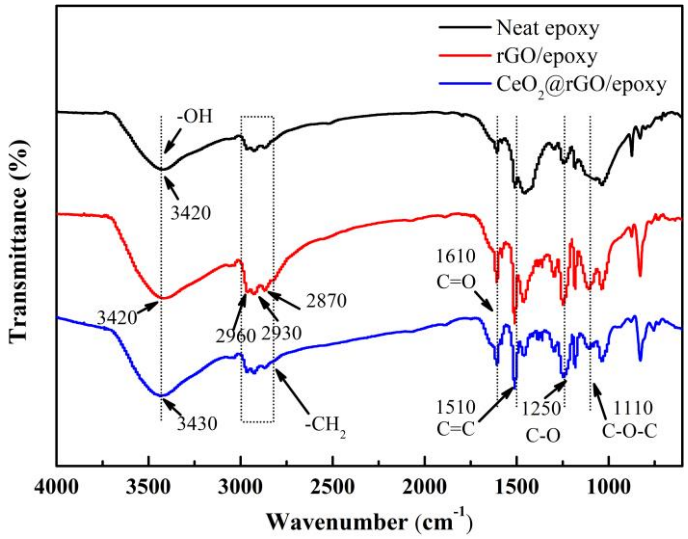
Neat epoxy
rGO/epoxy
CeO2@rGO/epoxy
-OH
3420
1610
C=O
2870
2960
2930
3420
3430
-CH2
1510
C=C
1250
C-O
1110
C-O-C
Transmittance (%)
Wavenumber (cm-1)

Fig. 4.

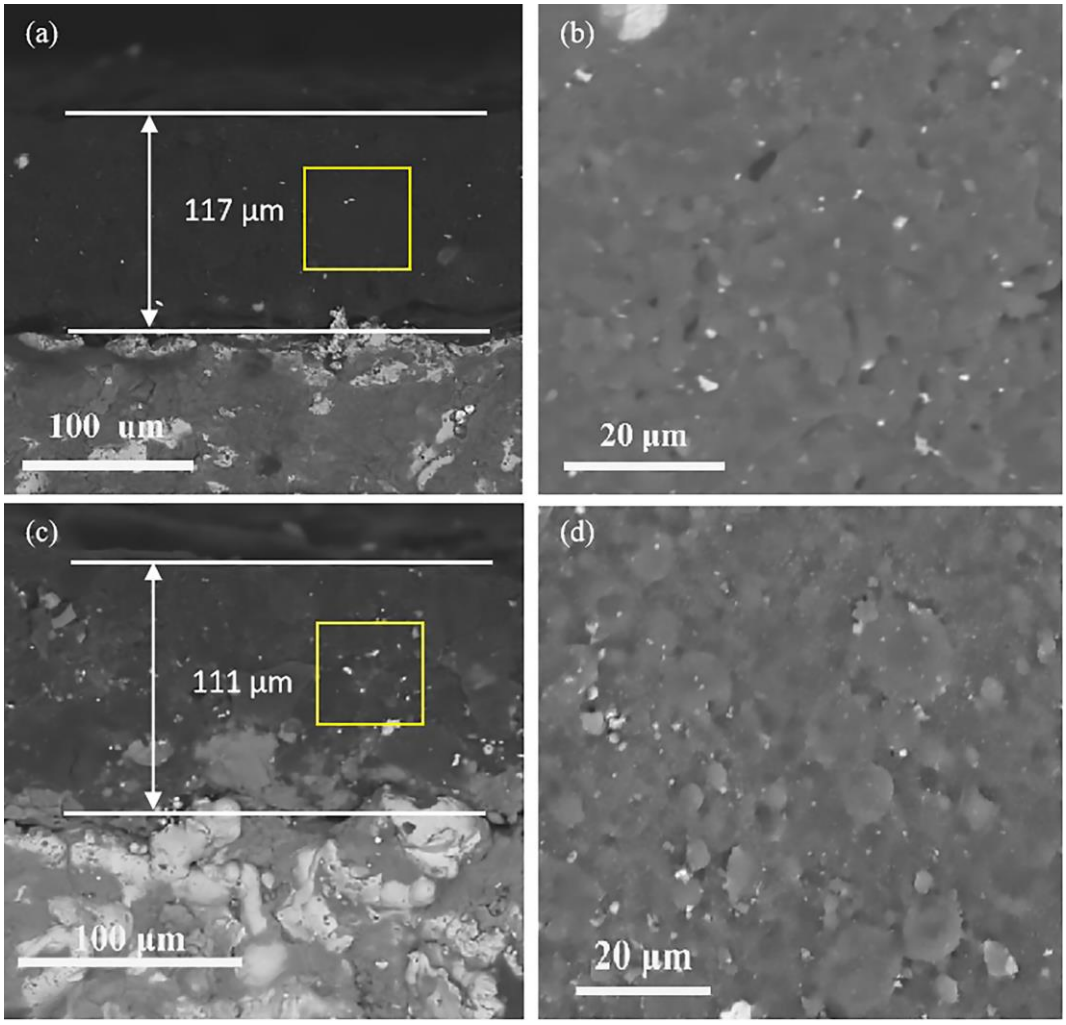

Fig. 5.

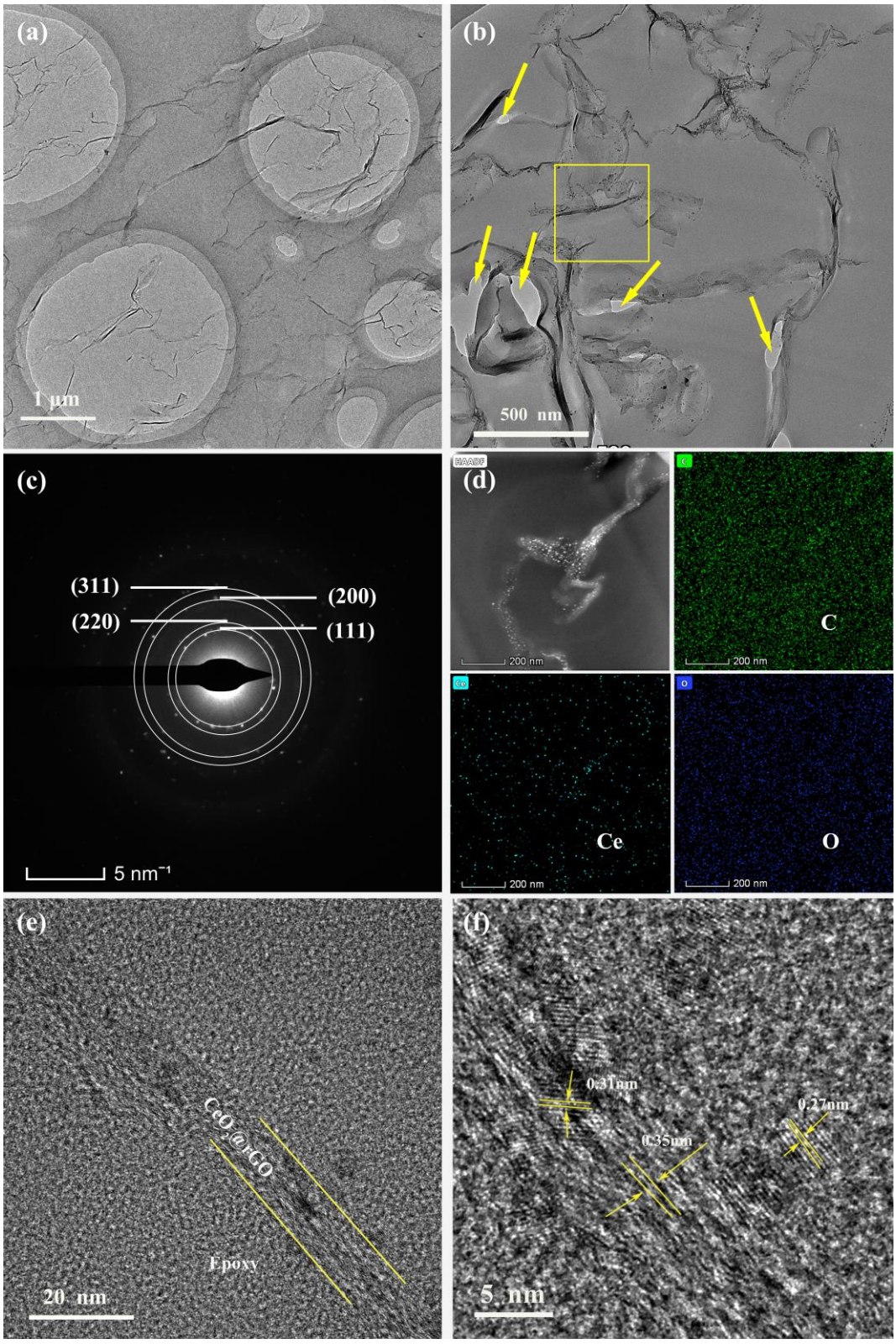
(a)
1 μm
(b)
500 nm
(c)
(311)
(200)
(220)
(111)
5 nm⁻¹
(d)
HAADF
C
Ce
O
200 nm
(e)
CeO2@rGO
Epoxy
20 nm
(f)
0.31nm
0.27nm
0.35nm
5 nm

Fig. 6.

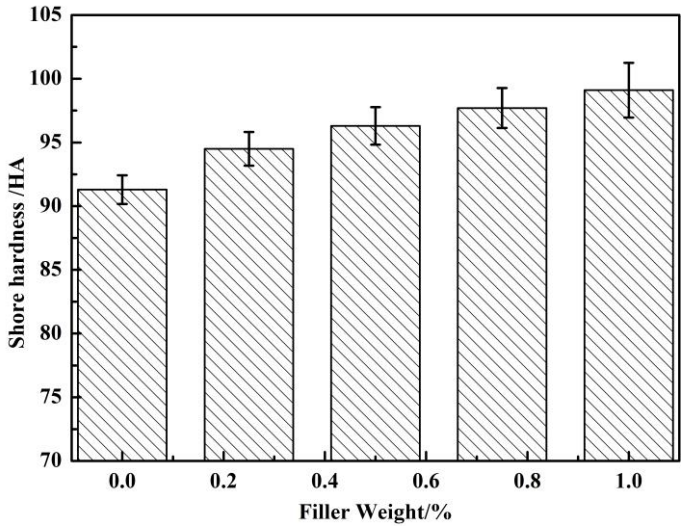
105
100
95
90
85
80
75
70
Shore hardness /HA
0.0
0.2
0.4
0.6
0.8
1.0
Filler Weight/%

Fig. 7.

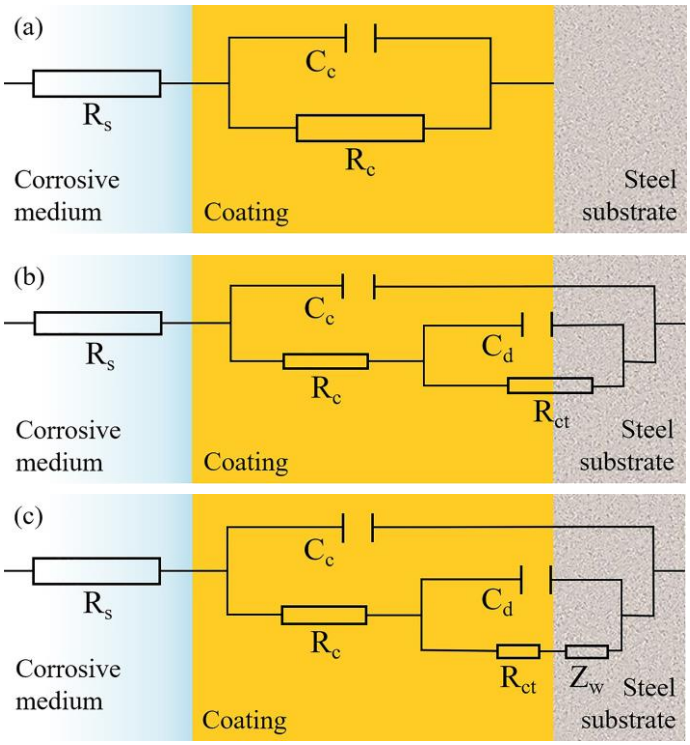
(a)
C_c
R_s
R_c
Corrosive medium
Coating
Steel substrate
(b)
C_c
C_d
R_s
R_c
R_{ct}
Corrosive medium
Coating
Steel substrate
(c)
C_c
C_d
R_s
R_c
R_{ct}
Z_w
Corrosive medium
Coating
Steel substrate

Fig. 8.

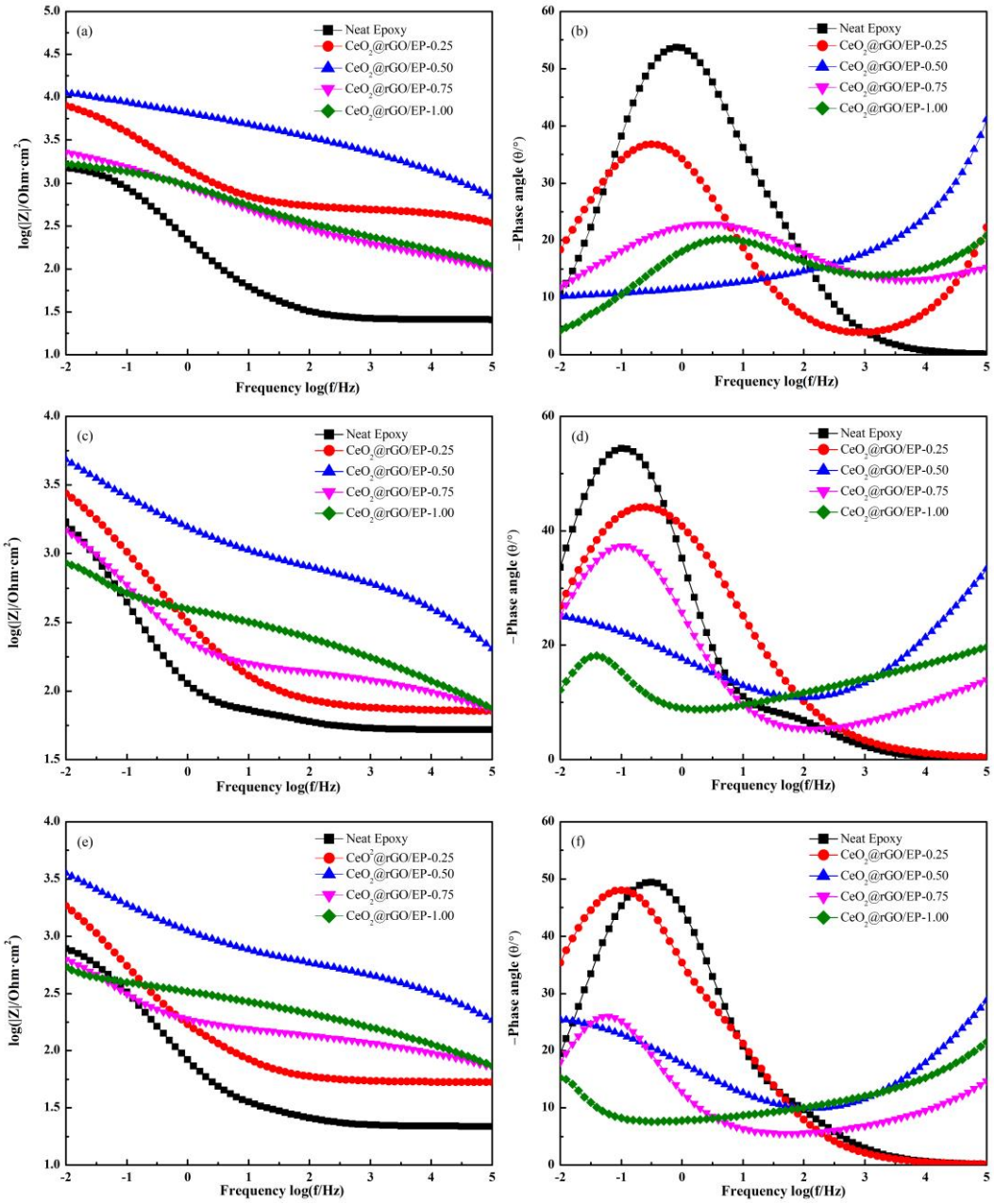
(a)
(b)
(c)
(d)
(e)
(f)
Neat Epoxy
CeO2@rGO/EP-0.25
CeO2@rGO/EP-0.50
CeO2@rGO/EP-0.75
CeO2@rGO/EP-1.00
log(|Z|/(Ohm·cm2))
−Phase angle (θ/°)
Frequency log(f/Hz)

Fig. 9.

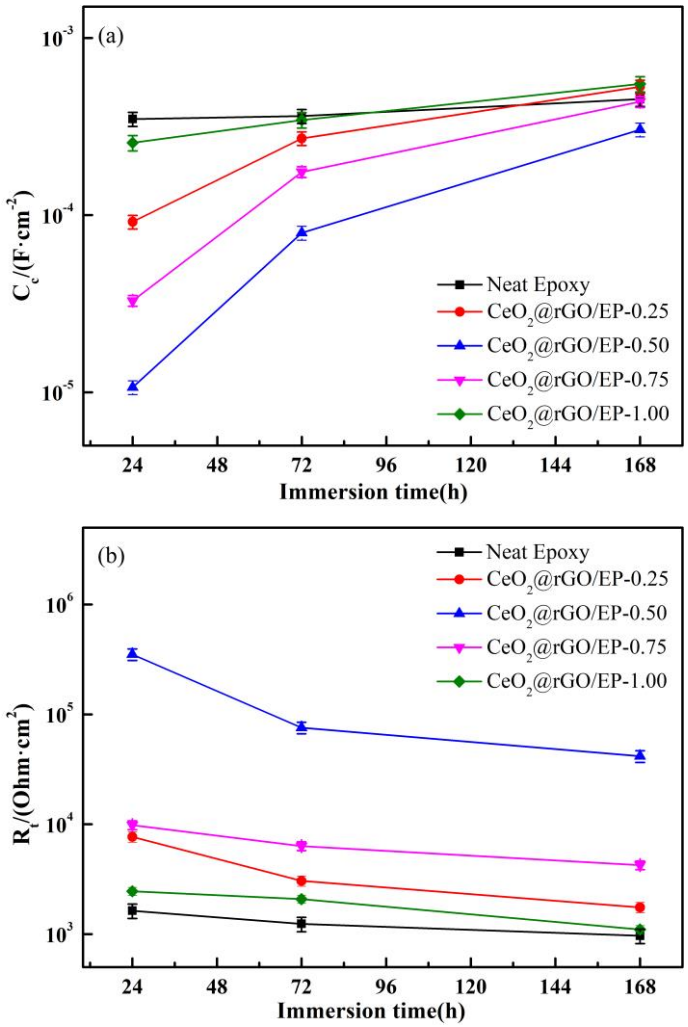
(a)
C_c/(F·cm^{-2})
Immersion time(h)
Neat Epoxy
CeO$_2$@rGO/EP-0.25
CeO$_2$@rGO/EP-0.50
CeO$_2$@rGO/EP-0.75
CeO$_2$@rGO/EP-1.00
(b)
R_t/(Ohm·cm^2)
Immersion time(h)
Neat Epoxy
CeO$_2$@rGO/EP-0.25
CeO$_2$@rGO/EP-0.50
CeO$_2$@rGO/EP-0.75
CeO$_2$@rGO/EP-1.00

Fig. 10.

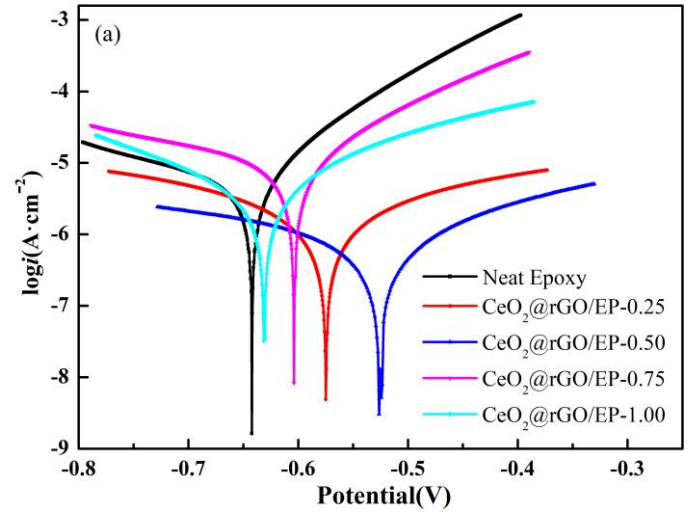
(a)
logi/(A·cm^{-2})
Potential(V)
Neat Epoxy
CeO$_2$@rGO/EP-0.25
CeO$_2$@rGO/EP-0.50
CeO$_2$@rGO/EP-0.75
CeO$_2$@rGO/EP-1.00

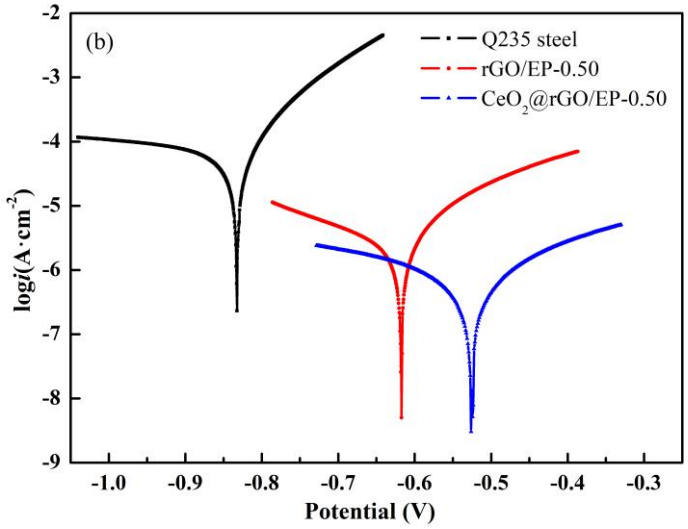
(b)
Q235 steel
rGO/EP-0.50
CeO2@rGO/EP-0.50
logi/(A·cm-2)
Potential (V)
-2
-3
-4
-5
-6
-7
-8
-9
-1.0
-0.9
-0.8
-0.7
-0.6
-0.5
-0.4
-0.3

Fig. 11.

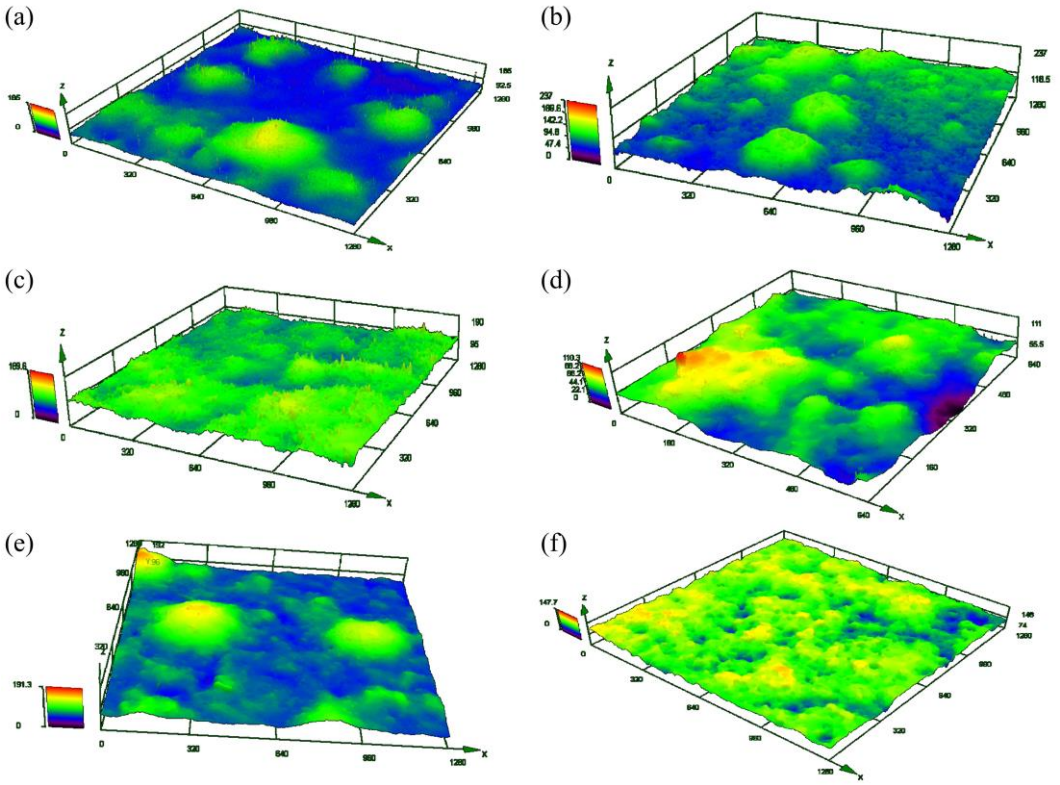
(a)
(b)
(c)
(d)
(e)
(f)

Fig. 12.

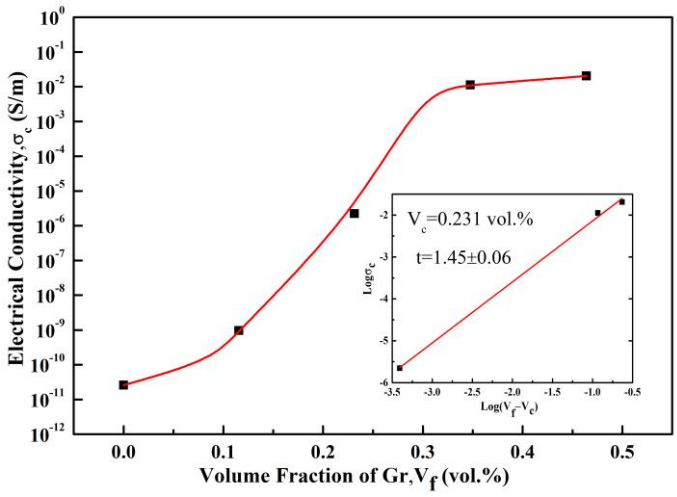
Electrical Conductivity,σc (S/m)
Volume Fraction of Gr,Vf (vol.%)
Vc=0.231 vol.%
t=1.45±0.06
Logσc
Log(Vf−Vc)

Fig. 13.